

# Deep Stochastic Mechanics

Elena Orlova <sup>\*1</sup>, Aleksei Ustimenko <sup>\*†2</sup>, Ruoxi Jiang<sup>1</sup>, Peter Y. Lu<sup>1</sup>, and Rebecca Willett<sup>1</sup>

<sup>1</sup>The University of Chicago, US

<sup>2</sup>ShareChat, UK

## Abstract

This paper introduces a novel deep-learning-based approach for numerical simulation of a time-evolving Schrödinger equation inspired by stochastic mechanics and generative diffusion models. Unlike existing approaches, which exhibit computational complexity that scales exponentially in the problem dimension, our method allows us to adapt to the latent low-dimensional structure of the wave function by sampling from the Markovian diffusion. Depending on the latent dimension, our method may have far lower computational complexity in higher dimensions. Moreover, we propose novel equations for stochastic quantum mechanics, resulting in linear computational complexity with respect to the number of dimensions. Numerical simulations verify our theoretical findings and show a significant advantage of our method compared to other deep-learning-based approaches used for quantum mechanics.

## 1 Introduction

Mathematical models for many problems in nature appear in the form of partial differential equations (PDEs) in high dimensions. Given access to precise solutions of the many-electron time-dependent Schrödinger equation (TDSE), a vast body of scientific problems could be addressed, including in quantum chemistry [1, 2], drug discovery [3, 4], condensed matter physics [5, 6], and quantum computing [7, 8]. However, solving high-dimensional PDEs and the Schrödinger equation, in particular, is a notoriously difficult problem in scientific computing due to the well-known curse of dimensionality: the computational complexity grows exponentially as a function of the dimensionality of the problem [9]. Traditional numerical solvers have been limited to dealing with problems in rather low dimensions since they rely on a grid.

Deep learning is a promising way to avoid the curse of dimensionality [10, 11]. However, no known deep learning approach avoids it in the context of the TDSE [12]. Although generic deep learning approaches have been applied to solving the TDSE [13, 14, 15, 16], this paper shows that it is possible to get performance improvements by developing an approach specific to the TDSE by incorporating quantum physical structure into the deep learning algorithm itself.

We propose an algorithm that relies on stochastic interpretation of quantum mechanics [17, 18, 19] and is inspired by the success of deep diffusion models that can model complex multi-dimensional distributions effectively [20]; we call it *Deep Stochastic Mechanics (DSM)*. Our approach is not limited to only the linear Schrödinger equation, but can be adapted to Klein-Gordon, Dirac equations [21, 22], and to the non-linear Schrödinger equations of condensed matter physics, e.g., by using mean-field stochastic differential equations (SDEs) [23], or McKean-Vlasov SDEs [24].

### 1.1 Problem formulation

The Schrödinger equation, a governing equation in quantum mechanics, predicts the future behavior of a dynamic system for  $0 \leq t \leq T$  and  $\forall x \in \mathcal{M}$ :

---

<sup>\*</sup>Main contribution.

<sup>†</sup>The corresponding author: research@aleksei.uk

$$i\hbar\partial_t\psi(x,t) = \mathcal{H}\psi(x,t), \quad (1)$$

$$\psi(x,0) = \psi_0(x), \quad (2)$$

where  $\psi : \mathcal{M} \times [0, T] \rightarrow \mathbb{C}$  is a wave function defined over a manifold  $\mathcal{M}$ , and  $\mathcal{H}$  is a self-adjoint operator acting on a Hilbert space of wave functions. For simplicity of future derivations, we consider a case of a spinless particle in  $\mathcal{M} = \mathbb{R}^{d1}$  moving in a smooth potential  $V : \mathbb{R}^d \times [0, T] \rightarrow \mathbb{R}_+$ . In this case,  $\mathcal{H} = -\frac{\hbar^2}{2}\text{Tr}(m^{-1}\nabla^2) + V$ , where  $m \in \mathbb{R}^d \otimes \mathbb{R}^d$  is a mass tensor. The probability density of finding a particle at position  $x$  is  $|\psi(x,t)|^2$ .

Given initial conditions in the form of samples drawn from a density  $\psi_0(x)$ , we wish to draw samples from  $|\psi(x,t)|^2$  for  $t \in (0, T]$  using a neural-network-based approach that can adapt to latent low-dimensional structure in the system and hence sidestep the curse of dimensionality. Rather than estimating  $\psi(x,t)$  explicitly and then sampling from the corresponding density, we devise a strategy that directly samples from  $|\psi(x,t)|^2$ , concentrating computation in regions of high density. When regions where the density  $|\psi(x,t)|^2$  lie in a latent low-dimensional space, our sampling strategy concentrates computation in that space, leading to the favorable scaling properties of our approach.

## 2 Related work

Physics-Informed Neural Networks (PINNs) [13] are general-purpose tools that have been widely studied for their ability to solve PDEs and can be applied to solve 1. However, this method is prone to the same issues as classical numerical algorithms since it relies on a collection of collocation points uniformly sampled over the domain  $\mathcal{M} \subseteq \mathbb{R}^d$ . In the remainder of the paper, we refer to this as a grid for simplicity of exposition. Another recent paper [25] introduces Neural Galerkin schemes based on deep learning, which leverage active learning to generate training data samples for numerically solving real-valued PDEs. Unlike collocation-points-based methods, this approach allows theoretically adaptive data collection guided by the dynamics of the equations if we could sample from the wave-function effectively.

Another family of approaches, FermiNet [26] or PauliNet [27], reformulates the problem (1) as maximization of an energy functional that depends on the solution of the stationary Schrödinger equation. This approach sidesteps the curse of dimensionality but cannot be adapted to the time-dependent wave function setting considered in this paper.

Our work brings a new perspective on what is a simulation of quantum mechanics. The only thing that we can experimentally obtain is samples from the quantum mechanics density. So, it makes sense to focus on obtaining samples from the density, rather than attempting to solve the Schrödinger equation; these samples can be used to make predictions about the system’s behavior without conducting real-world experiments. Based on this observation, there are a variety of quantum Monte Carlo methods [28, 29, 30], which rely on estimating expectations of observables rather than the wave function itself, resulting in improved computational efficiency. However, these methods still encounter the curse of dimensionality due to recovering the full density operator. The density operator in atomic simulations is concentrated on a lower dimensional manifold of such operators [23], suggesting that methods which adapt to this manifold can be more effective than high-dimensional grid-based methods. Deep learning has the ability to adapt to this structure.

As noted in [31], knowledge of the density is unnecessary for sampling. We need a score function  $\nabla \log \rho$  to be able to sample from it. The fast-growing field of generative modeling with diffusion processes demonstrates that for high-dimensional densities with low-dimensional manifold structure, it is incomparably more effective to learn a score function than the density itself [32, 20].

For high-dimensional real-valued PDEs, there exist a variety of classic and deep learning-based approaches that rely on sampling from diffusion processes, e.g., [33, 34, 16, 15]. Those works rely on the Feynman-Kac formula [35] to obtain an estimator for the solution to the PDE. However, for the Schrödinger equation, we need an analytical continuation of the Feynman-Kac formula on an imaginary time axis [36] as it is a complex-valued equation. This requirement limits the applicability of this approach to our setting.

---

<sup>1</sup>A multi-particle case is covered by considering  $d = 3n$ , where  $n$  – the number of particles.

### 3 Contributions

We are inspired by works of Nelson [17, 19], who has developed a stochastic interpretation of quantum mechanics, so-called stochastic mechanics, based on a Markovian diffusion. Instead of solving the Schrödinger equation (1), our method aims to learn the stochastic mechanical process’s osmotic and current velocities equivalent to classical quantum mechanics. Our formulation differs from the original one [17, 19, 18], as we derive differential equations describing the velocities that do not require the computation of the Laplacian operator. Another difference is that our formulation interpolates anywhere between stochastic mechanics and deterministic Pilot-wave theory [37]. More details are given in Appendix F.2.

We highlight the main contributions of this work as follows:

- We propose to use a stochastic formulation of quantum mechanics [19, 17, 18] to create an efficient computational tool for quantum mechanics simulation. Our approach relies on Markovian diffusion and has polynomial time and memory complexity in the problem dimension, while classical numerical solvers and other ML approaches scale exponentially since they usually rely on a grid. We develop a new algorithm for learning the forward and backward diffusion drifts that are parametrized via neural networks.
- We also derive equations describing stochastic mechanics that are equivalent to the expressions introduced by Nelson but which are expressed in terms of the gradient of the divergence operator, making them more amenable to neural network-based solvers. This enables us to reduce further the computational complexity of computing the loss from quadratic to linear in the dimension.
- We empirically estimate the performance of our method in various settings. Our approach shows a superior advantage to PINNs in terms of accuracy. For example, in the case of a 1d harmonic oscillator, we gain 89 % of improvement on the averaged mean error rates compared with the PINN. We also conduct an experiment where our method shows linear convergence time in the dimension, operating easily in higher-dimensional harmonic oscillators where our computing systems cannot store the grid necessary for PINNs or classical methods.

Table 1 compares properties of methods for solving (1), where  $N$  is the number of discretization points in time, and  $M_d$  is the number of Monte Carlo iterations required by FermiNet to draw a single sample. We follow the general recommendation that the number of points on the grid for each spatial dimension should be  $\sqrt{N}$ . Thus, the number of points on a grid should be  $\mathcal{O}(N^{\frac{d}{2}+1})$ . Approaches like the PINN or FermiNet require computing the Laplacian, which leads to at least quadratic computational complexity per iteration. The PINNs approach cannot adapt to the latent low-dimensional structure as effectively as FermiNet does.

Table 1: Comparison of different approaches for simulating quantum mechanics.

Method	Domain	Time-evolving	Adaptive	Iteration Complexity
PINN ([13])	Compact	✓	✗	$\mathcal{O}(d^2)$
FermiNet ([26])	$\mathbb{R}^d$	✗	✓	$\mathcal{O}(d^2 M_d)^2$
Finite-difference	Compact	✓	✗	$\mathcal{O}(N^{\frac{d}{2}+1})$
<b>DSM (Ours)</b>	$\mathbb{R}^d$	✓	✓	$\mathcal{O}(dN)$

While our approach may or may not be able to solve effectively complex multi-particle simulations as it is, we view our work as a foundational step towards future advancements. We deliberately keep our algorithm and neural architecture as simple as possible to prove the concept that our framework works. Our primary objective is to address the fundamental issues associated with simulating quantum mechanics.

<sup>2</sup>Although the original method is for Bohr-Openheimer potential that leads to even higher complexity, we do not take this into account here.

## 4 Stochastic processes of quantum mechanics

There is a family of diffusion processes that are equivalent to Equation (1) in a sense that all time-marginals of any such process coincide with  $|\psi|^2$ ; we refer to Appendix E for derivation. Assuming  $\psi(x, t) = \sqrt{\rho(x, t)}e^{iS(x, t)}$ , we define:

$$v(x, t) = \frac{\hbar}{m} \nabla S(x, t) \quad \text{and} \quad u(x, t) = \frac{\hbar}{2m} \nabla \log \rho(x, t). \quad (3)$$

Our method uses the following stochastic process for our method with  $\nu \geq 0$ <sup>3</sup>, which corresponds to sampling from  $\rho = |\psi(x, t)|^2$ :

$$dX(t) = (v(X(t), t) + \nu u(X(t), t))dt + \sqrt{\frac{\nu \hbar}{m}} dW(t), \quad (4)$$

$$X(0) \sim |\psi_0|^2, \quad (5)$$

where  $u$  is an osmotic velocity,  $v$  is a current velocity and  $W(t)$  is a standard Wiener process. Any numerical integrator can be used to obtain samples from the diffusion process. The simplest one is the Euler-Maruyama integrator [38]:

$$X_{i+1} = X_i + (v(X_i, t_i) + \nu u(X_i, t_i))\epsilon + \mathcal{N}(0, \frac{\nu \hbar}{m} \epsilon I_d), \quad (6)$$

where  $\epsilon > 0$  denotes a step size,  $0 \leq i < \frac{T}{\epsilon}$ , and  $\mathcal{N}(0, I_d)$  is a Gaussian distribution. We consider this integrator in our work. Switching to higher-order integrators, e.g., the Runge-Kutta family of integrators [38], can potentially enhance efficiency and stability when  $\epsilon$  is larger.

### 4.1 Stochastic mechanics

The diffusion process (4) achieves sampling from  $\rho = |\psi(x, t)|^2$  for each  $t \in [0, T]$  for known  $u$  and  $v$ ; our approach learns neural networks to represent those velocities. Assume that  $\psi_0 = \sqrt{\rho_0}e^{iS_0}$ . Our approach relies on the following equations for the velocities:

$$\partial_t v = -\frac{1}{m} \nabla V + \langle u, \nabla \rangle u - \langle v, \nabla \rangle v + \frac{\hbar}{2m} \nabla \langle \nabla, u \rangle, \quad (7a)$$

$$\partial_t u = -\nabla \langle v, u \rangle - \frac{\hbar}{2m} \nabla \langle \nabla, v \rangle, \quad (7b)$$

$$v_0(x) = \frac{\hbar}{m} \nabla S_0(x), \quad u_0(x) = \frac{\hbar}{2m} \nabla \log \rho_0(x). \quad (7c)$$

These equations are derived in Appendix F and are equivalent to the Schrödinger equation. As mentioned before, our equations are different from the canonical ones developed in [17, 18]. In particular, the original formulation, which we call *Nelsonian version*, uses the Laplacian of  $u$  in Equation (7a). *Our version* replaces it with the gradient of the divergence operator.

## 5 Deep Stochastic Mechanics (DSM)

Although PINNs can be used to solve the equations (7a), (7b), that approach would suffer from the curse of dimensionality. Recall the SDE associated with the Schrödinger equation:

$$dX(t) = (v(X(t), t) + \nu u(X(t), t))dt + \sqrt{\frac{\nu \hbar}{m}} dW(t). \quad (8)$$

The core idea of our approach is to minimize the error of equations (7a), (7b) on sample trajectories  $X(t)$  from the SDE. It allows our method to focus only on high-density regions and alleviates the inherent curse of dimensionality that comes from reliance on a grid. Moreover, this on-the-fly generation of the training data allows us to effectively adapt to the latent low-dimensional structure of the wave function without explicitly incorporating any prior knowledge into the algorithm.

<sup>3</sup> $\nu = 0$  is allowed if and only if  $\psi_0$  is sufficiently regular, e.g.,  $|\psi_0|^2 > 0$  everywhere.

## 5.1 Learning drifts

This section describes how we learn the velocities  $u(X, t) = u_\theta(X, t)$  and  $v(X, t) = v_\theta(X, t)$ , parameterized by neural networks with parameters  $\theta$ . We propose to use a combination of three losses: two of them come from the Navier-Stokes-like equations (7a), (7b), and the third one enforces the initial conditions (7c). We define non-linear differential operators that appear in Equation (7a), (7b):

$$\mathcal{D}_u[v, u, x, t] = -\nabla \langle v(x, t), u(x, t) \rangle - \frac{\hbar}{2m} \nabla \langle \nabla, v(x, t) \rangle, \quad (9)$$

$$\mathcal{D}_v[v, u, x, t] = \frac{1}{m} \nabla V(x, t) + \frac{1}{2} \nabla \|u(x, t)\|^2 - \frac{1}{2} \nabla \|v(x, t)\|^2 + \frac{\hbar}{2m} \nabla \langle \nabla, u(x, t) \rangle \quad (10)$$

We aim to minimize the following losses:

$$L^u(\theta) = \mathbb{E}_{t \sim U[0, T]} \mathbb{E}_{x \sim \rho(\cdot, t)} \|\partial_t u_\theta(x, t) - \mathcal{D}_u[v_\theta, u_\theta, x, t]\|^2, \quad (11)$$

$$L^v(\theta) = \mathbb{E}_{t \sim U[0, T]} \mathbb{E}_{x \sim \rho(\cdot, t)} \|\partial_t v_\theta(x, t) - \mathcal{D}_v[v_\theta, u_\theta, x, t]\|^2, \quad (12)$$

$$L^0(\theta) = \mathbb{E}_{x \sim |\psi_0|^2} (\|u_\theta(x, 0) - u_0(x)\|^2 + \|v_\theta(x, 0) - v_0(x)\|^2) \quad (13)$$

where  $u_0, v_0$  are defined in Equation (7c). Finally, we define a combined loss using weighted sum with  $w_u, w_v, w_0 > 0$ :

$$\mathcal{L}(\theta) = w_u L^u(\theta) + w_v L^v(\theta) + w_0 L^0(\theta). \quad (14)$$

The basic idea of our approach is to, for each iteration  $\tau$ , to sample new trajectories using Equation (6) with  $\nu = 1$ . These trajectories are then used to compute stochastic estimates of the loss (14), and then we back-propagate gradients of the loss to update  $\theta$ . We re-use recently generated trajectories to reduce computational overhead as SDE integration cannot be paralleled. The training procedure is summarized in Algorithm 1 and Figure 1; a more detailed version is presented in Appendix B.

---

### Algorithm 1 A training algorithm pseudo-code

---

**Input**  $\psi_0$  – initial wave-function,  $M$  – epoch number,  $B$  – batch size, other parameters (optimizer parameters, physical constants, Euler-Maryama parameters; see Appendix B)  
Initialize NNs  $u_{\theta_0}, v_{\theta_0}$   
**for** each iteration  $0 \leq \tau < M$  **do**  
    Sample  $B$  trajectories  
    using  $u_{\theta_\tau}, v_{\theta_\tau}$  via Equation (6) with  $\nu = 1$   
    Estimate loss  $\mathcal{L}(\theta_\tau)$  from Equation (14) over the sampled trajectories  
    Back-propagate gradients to get  $\nabla_\theta \mathcal{L}(\theta_\tau)$   
    Adam optimizer step to get  $\theta_{\tau+1}$   
**end for**  
**output**  $u_{\theta_M}, v_{\theta_M}$

---

We can use trained  $u_{\theta_M}, v_{\theta_M}$  to simulate the forward diffusion for  $\nu \geq 0$  given  $X_0 \sim \mathcal{N}(0, I_d)$ :

$$X_{i+1} = X_i + (v_{\theta_M}(X_i, t_i) + \nu u_{\theta_M}(X_i, t_i))\epsilon + \mathcal{N}\left(0, \frac{\hbar}{m} \nu \epsilon I_d\right). \quad (15)$$

In Appendix H, we describe a wide variety of possible ways to apply our approach for estimating arbitrary quantum observable  $\mathbf{Y}$ , singular initial conditions like  $\psi_0 = \delta_{x_0}$ , singular potentials, correct estimations of observable that involve measurement process, recovering the wave function from  $u, v$ .

## 5.2 On convergence

We use Adam optimizer [39] in our experiments. Since the operators (9) are not linear, we may not be able to claim convergence to the global optima of such methods as SGD or Adam in the Neural Tangent Kernel (NTK) [40] limit. Such proof exists for PINNs in [41] due to the linearity of the Schrödinger equation (1). It is possible that non-linearity in the loss (14) requires non-convex methods to achieve theoretical guarantees on convergence to the global optima, e.g., [42, 43]. Further research into NTK and non-linear PDEs is needed [41].

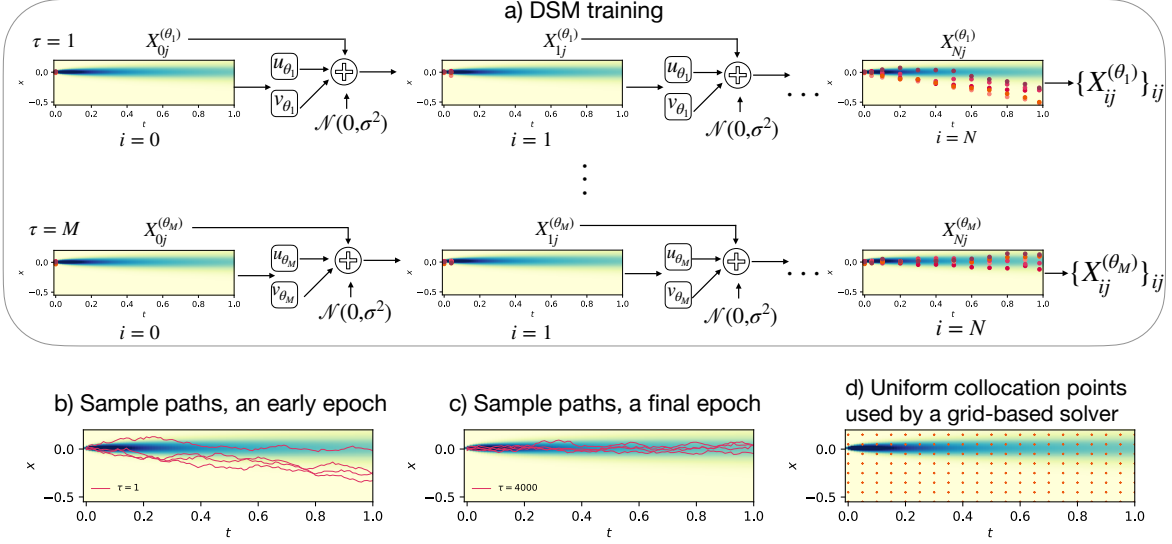


Figure 1: An illustration of our approach. Blue regions in the plots correspond to higher-density regions. (a) DSM training scheme: at every epoch  $\tau$ , we generate  $B$  full trajectories  $\{X_{ij}\}_{ij}$ ,  $i = 0, \dots, N$ ,  $j = 1, \dots, B$ . Then we update the weights of our NNs. (b) An illustration of sampled trajectories at the early epoch. (c) An illustration of sampled trajectories at the final epoch. (d) Collocation points for a grid-based solver where it should predict values of  $\psi(x, t)$ .

The only source of noise in our loss (14) comes from trajectory sampling. This fact is in sharp contrast with generative diffusion models relying on score matching [20]. In these models, the loss has  $\mathcal{O}(\epsilon^{-1})$  variance as it attempts to numerically estimate the stochastic differential  $\frac{X(t+\epsilon) - X(t)}{\sqrt{\epsilon}}$  which leads to  $\frac{1}{\sqrt{\epsilon}}$  contribution from increments of the Wiener process. In our loss, the stochastic differentials are evaluated analytically in Equation (9) avoiding such contributions; for details see [17, 19]. This leads  $\mathcal{O}(1)$  variance of the gradient and, thus, allows us to achieve fast convergence with smaller batches.

## 6 Experiments

**Experimental setup:** As a baseline, we use an analytical solution (if it is known) or a numerical solution. We compare our method’s (DSM) performance with PINNs when possible. Further details on architecture, training procedures, hyperparameters for our approach and PINNs, and numerical solvers can be found in Appendix C. The code of our experiments can be found on GitHub.<sup>4</sup>

**Evaluation metrics:** We estimate errors between the true values of the mean and the variance of  $X_t$  as the relative  $L_2$ -norm, namely  $\mathcal{E}_m(X_i)$  and  $\mathcal{E}_v(X_i)$ . The standard deviation (confidence intervals) of the observables are indicated in the results. True  $v$  and  $u$  values are estimated numerically with the finite difference method. Our trained  $u_\theta$  and  $v_\theta$  should output these values. We measure errors  $\mathcal{E}(u)$  and  $\mathcal{E}(v)$  as the  $L_2$ -norm between the true and predicted values in  $L_2(\mathbb{R}^d \times [0, T], \mu)$  with  $\mu(dx, dt) = \frac{1}{T} |\psi(x, t)|^2 dx dt$ .

### 6.1 Singular initial conditions

As a proof of concept, we consider a case of one particle  $x \in \mathbb{R}^1$  with  $V(x) \equiv 0$  and  $\psi_0 = \delta_0$ ,  $t \in [0, 1]$ . Since  $\delta$ -function is a generalized function, we must take a  $\delta$ -sequence for the training. The most straightforward approach is to take  $\tilde{\psi}_0 = \frac{1}{(2\pi\alpha)^{\frac{1}{4}}} e^{-\frac{x^2}{4\alpha}}$  with  $\alpha \rightarrow 0_+$ . In our experiments we take  $\alpha = \frac{\hbar^2}{m^2}$ , yielding  $v_0(x) \equiv 0$  and  $u_0(x) = -\frac{\hbar x}{2m\alpha}$ . Since  $\psi_0$  is singular, we must set  $\nu = 1$  during

<sup>4</sup><https://github.com/elena-orlova/deep-stochastic-mechanics>

sampling. The analytical solution is given as  $\psi(x, t) = \frac{1}{(2\pi t)^{\frac{1}{4}}} e^{-\frac{x^2}{4t}}$ . So, we expect the standard deviation of  $X(t)$  to grow as  $\sqrt{t}$ , and the mean value of  $X(t)$  to be zero.

We do not compare our approach with PINNs since it is a simple proof of concept, and the analytical solution is known. Figure 2 summarizes the results of our experiment. Specifically, the left panel of the figure shows the magnitude of the density obtained with our approach alongside the true density. The right panel of Figure 2 shows statistics of  $X_t$ , such as mean and variance, and the corresponding error bars. The resulting prediction errors are calculated against the truth data for this problem and are measured at  $0.008 \pm 0.007$  in the  $L_2$ -norm for the averaged mean and  $0.011 \pm 0.007$  in the relative  $L_2$ -norm for the averaged variance of  $X_t$ . Our approach can accurately capture the behavior of the Schrödinger equation in the singular initial condition case.

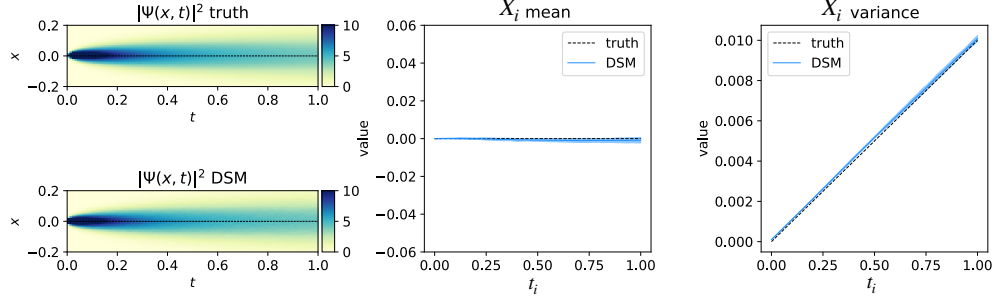


Figure 2: Results for the singular initial condition case. DSM corresponds to our method.

## 6.2 Harmonic oscillator

### 6.2.1 One-dimensional case

We consider a harmonic oscillator model with  $x \in \mathbb{R}^1$ ,  $V(x) = \frac{(x-0.1)^2}{2}$ ,  $t \in [0, 1]$ . The initial wave function is given as  $\psi(x, 0) \propto e^{-\frac{x^2}{4\sigma^2}}$ . Then  $u_0(x) = -\frac{\hbar x}{2m\sigma^2}$ ,  $v_0(x) \equiv 0$ .  $X(0)$  comes from  $X(0) \sim \mathcal{N}(0, \sigma^2)$ , where  $\sigma^2 = 0.1$ .

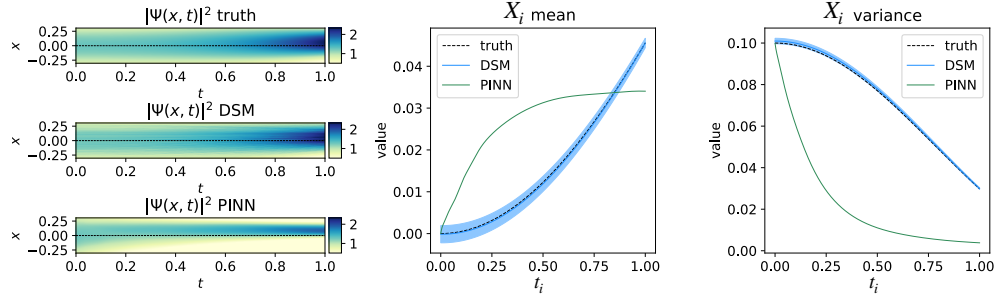
We use the numerical solution as the ground truth. Our approach is compared with a PINN. The PINN input data consists of  $N_0 = 1000$  data points sampled for estimating  $\psi(x, 0)$ ,  $N_b = 300$  data points for enforcing the boundary conditions (we assume zero boundary conditions), and  $N_f = 60000$  collocation points to enforce the corresponding equation inside the solution domain, all points sampled uniformly for  $x \in [-2, 2]$  and  $t \in [0, 1]$ .

Figure 3 (a) summarizes the results of our experiment. The left panel of the figure illustrates the evolution of the density  $|\psi(x, t)|^2$  over time for different methods. It is evident that our approach accurately captures the density evolution, while the PINN model initially aligns with the ground truth but deviates from it over time. Sampling collocation points uniformly when density is concentrated in a small region explains why PINN struggles to learn the dynamics of Equation (1); we illustrate this effect in Figure 1 (d).

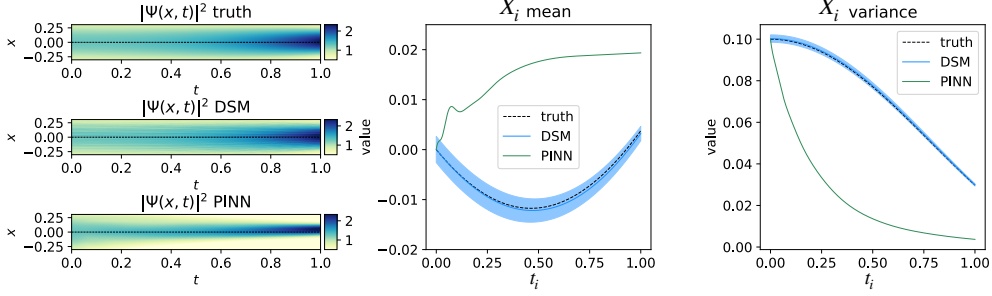
The right panel demonstrates observables of the system, the averaged mean of  $X_t$  and the averaged variance of  $X_t$ . Our approach consistently follows the corresponding distribution of  $X_t$ . On the contrary, the predictions of the PINN model only match the distribution at the initial time steps but fail to accurately represent it as time elapses. Table 2 shows the error rates and the training time for our method and PINNs. In particular, our method shows better performance in terms of all error rates compared to the PINN. These findings emphasize the better performance of the proposed method in capturing the dynamics of the Schrödinger equation compared to the PINN model.

We also consider a non-zero initial phase  $S_0(x) = -5x$ . It corresponds to the initial impulse of a particle. Then  $v_0(x) \equiv -\frac{5\hbar}{m}$ . The PINN inputs are  $N_0 = 3000$ ,  $N_b = 300$  data points, and  $N_f = 80000$  collocation points. Figure 3 (b) and Table 2 present the results of our experiment. Our method consistently follows the corresponding ground truth while the PINN model fails to do so. It indicates the ability of our method to accurately model the behavior of the quantum system.





(a) The harmonic oscillator with  $S_0(x) \equiv 0$ .



(b) The harmonic oscillator with  $S_0(x) = -5x$ .

Figure 3: The results for 1d harmonic oscillator. DSM corresponds to our method.

Table 2: The results for different harmonic oscillator settings. In the 3d setting, the reported errors are averaged across the dimensions. The **best** result is in bold.

Problem	Model	$\mathcal{E}_m(X_i) \downarrow$	$\mathcal{E}_v(X_i) \downarrow$	$\mathcal{E}(v) \downarrow$	$\mathcal{E}(u) \downarrow$	Train time
1d, $S_0(x) \equiv 0$	PINN	0.698	0.701	25.861	3.621	2h 9m
	DSM	<b>0.077 ± 0.052</b>	<b>0.011 ± 0.006</b>	<b>0.00011</b>	<b>2.811 × 10<sup>-5</sup></b>	45m 3s
1d, $S_0(x) = -5x$	PINN	2.819	0.674	281.852	68.708	3h 23m
	DSM	<b>0.223 ± 0.207</b>	<b>0.009 ± 0.008</b>	<b>1.645 × 10<sup>-5</sup></b>	<b>2.168 × 10<sup>-5</sup></b>	1h 45m
3d, $S_0(x) \equiv 0$	PINN (intractable)	—	—	—	—	—
	DSM (Nelsonian)	0.100 ± 0.061	0.012 ± 0.009	1.200 × 10 <sup>-4</sup>	<b>3.324 × 10<sup>-5</sup></b>	1h 48m
	DSM (Grad. Divergence)	<b>0.073 ± 0.048</b>	<b>0.011 ± 0.008</b>	<b>4.482 × 10<sup>-5</sup></b>	4.333 × 10 <sup>-5</sup>	2h 07m

### 6.2.2 Three-dimensional case

We further explore our approach by considering the harmonic oscillator model with  $S_0(x) \equiv 0$  with three non-interacting particles. This setting can be viewed as a 3d problem, where the solution is a 1d solution repeated three times. Due to computational resource limitations, we are unable to execute the PINN model. The number of collocation points should grow exponentially with the problem dimension so that the PINN model converges. We have about 512 GB of memory but cannot store 60000<sup>3</sup> points. We conduct experiments comparing two versions of the proposed algorithm: the Nelsonian one and our version.

Table 2 provides the quantitative results of these experiments. Our version demonstrates slightly better performance compared to the Nelsonian version, although the difference is not statistically significant. Empirically, our version requires more steps to converge compared to the Nelsonian version: 7000 vs. 9000 epochs correspondingly. However, the training time of the Nelsonian approach is about 20 mins longer than our approach's time. More illustrations and error rates across the dimensions can be found in Appendix D.1.



### 6.3 Algorithmic complexity

We measure the training time per epoch for two versions of the DSM algorithm for  $d = 1, 3, 5, 7, 9$ : the Nelsonian one and our version. The experiments are conducted using the harmonic oscillator model with  $S_0(x) \equiv 0$ . The results are averaged across 30 runs. Figure 4 on the left shows the results. It demonstrates quadratic time per iteration scaling for the Nelsonian version, while the time grows linearly for our version. The memory complexity results are given in Appendix D.2.

Figure 4 on the right illustrates the total training time versus the problem dimension. We train our models until the training loss reaches a threshold of  $2.5 \times 10^{-5}$ . We observe that train time grows linearly with  $d$ . The performance errors are presented in Appendix D.2. These empirical findings demonstrate the computational efficiency of our algorithm. In contrast, traditional numerical solvers would suffer from exponential growth in data when tackling this task.

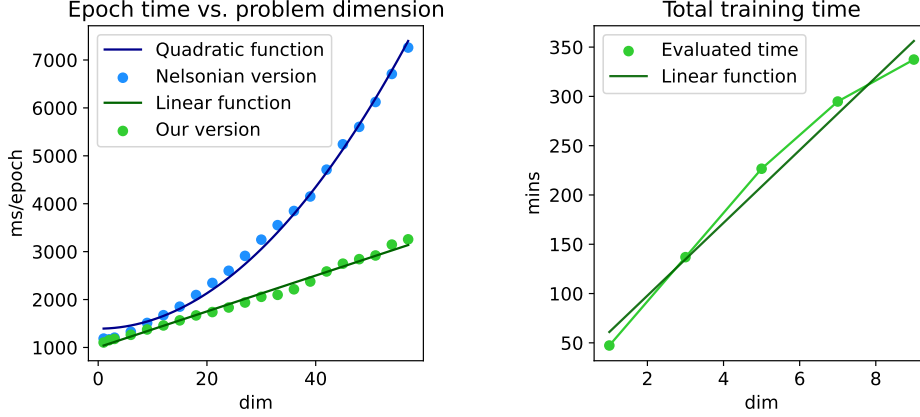


Figure 4: Results for the singular initial condition case. DSM corresponds to our method.

## 7 Discussion

**Limitations:** This paper considers the simplest case of the linear spinless Schrödinger equation on a flat manifold  $\mathbb{R}^d$  with a smooth potential. For many practical setups, such as quantum chemistry, quantum computing or condensed matter physics, our approach should be modified, e.g., by adding a spin component or by considering some approximation and, therefore, requires additional validations that are beyond of the scope of this work. We have shown evidence of adaptation of our method to one kind of low-dimensional structure, but this paper does not explore a broader range of systems with low latent dimension.

**Broader impacts:** It is hypothesized that simulations of quantum systems cannot be done effectively on classic computers, otherwise known as the problem of  $P \neq BQP$  [44]. If that is true, then no algorithms should scale as a polynomial of the dimension for *all* problems. In our work, we propose the algorithm that can simulate *some* systems effectively in linear time. It may be possible to learn polynomial-time approximations to Shor’s algorithm [45] on a classic computer using some modification of the proposed deep learning approach. While this possibility is highly unlikely, the risk that comes with it [46] should not be ignored.

## 8 Conclusion

We develop the new algorithm for simulating quantum mechanics that addresses the curse of dimensionality by leveraging the latent low-dimensional structure of the system. This approach is based on a modification of the stochastic mechanics theory that establishes a correspondence between the Schrödinger equation and a diffusion process. We learn the drifts of this diffusion process using deep learning to sample from the corresponding quantum density. We believe that our approach has the

potential to bring to quantum mechanics simulation the same progress that deep learning has enabled in artificial intelligence. We provide extensive future work discussion in [Appendix I](#).

## 9 Acknowledgments

The authors gratefully acknowledge the support of DOE grant DE-SC0022232, AFOSR grant FA9550-18-1-0166, and NSF grants DMS-2023109 and DMS-1925101. Peter Y. Lu gratefully acknowledges the support of the Eric and Wendy Schmidt AI in Science Postdoctoral Fellowship, a Schmidt Futures program.

## References

- [1] Eric Cancès, Mireille Defranceschi, Werner Kutzelnigg, Claude Le Bris, and Yvon Maday. Computational quantum chemistry: a primer. *Handbook of numerical analysis*, 10:3–270, 2003.
- [2] Hiroshi Nakatsuji. Discovery of a general method of solving the Schrödinger and Dirac equations that opens a way to accurately predictive quantum chemistry. *Accounts of Chemical Research*, 45(9):1480–1490, 2012.
- [3] Aravindh Ganeshan, Michelle L Coote, and Khaled Barakat. Molecular dynamics-driven drug discovery: leaping forward with confidence. *Drug discovery today*, 22(2):249–269, 2017.
- [4] Alexander Heifetz. *Quantum mechanics in drug discovery*. Springer, 2020.
- [5] Rong-Xiang Liu, Bo Tian, Li-Cai Liu, Bo Qin, and Xing Lü. Bilinear forms, n-soliton solutions and soliton interactions for a fourth-order dispersive nonlinear Schrödinger equation in condensed-matter physics and biophysics. *Physica B: Condensed Matter*, 413:120–125, 2013.
- [6] Bruce M Boghosian and Washington Taylor IV. Quantum lattice-gas model for the many-particle Schrödinger equation in d dimensions. *Physical Review E*, 57(1):54, 1998.
- [7] Lov K Grover. From Schrödinger’s equation to the quantum search algorithm. *Pramana*, 56:333–348, 2001.
- [8] Anargyros Papageorgiou and Joseph F Traub. Measures of quantum computing speedup. *Physical Review A*, 88(2):022316, 2013.
- [9] Richard E Bellman. *Dynamic programming*. Princeton university press, 2010.
- [10] Tomaso Poggio, Hrushikesh Mhaskar, Lorenzo Rosasco, Brando Miranda, and Qianli Liao. Why and when can deep-but not shallow-networks avoid the curse of dimensionality: a review. *International Journal of Automation and Computing*, 14(5):503–519, 2017.
- [11] Vamshi C Madala, Shivkumar Chandrasekaran, and Jason Bunk. CNNs avoid curse of dimensionality by learning on patches. *IEEE Open Journal of Signal Processing*, 2023.
- [12] Sergei Manzhos. Machine learning for the solution of the Schrödinger equation. *Machine Learning: Science and Technology*, 1(1):013002, 2020.
- [13] Maziar Raissi, Paris Perdikaris, and George E Karniadakis. Physics-informed neural networks: A deep learning framework for solving forward and inverse problems involving nonlinear partial differential equations. *Journal of Computational physics*, 378:686–707, 2019.
- [14] Weinan E and Bing Yu. The deep ritz method: A deep learning-based numerical algorithm for solving variational problems, 2017.
- [15] E Weinan, Jiequn Han, and Arnulf Jentzen. Algorithms for solving high dimensional PDEs: from nonlinear Monte Carlo to machine learning. *Nonlinearity*, 35(1):278, 2021.
- [16] Jiequn Han, Arnulf Jentzen, and Weinan E. Solving high-dimensional partial differential equations using deep learning. *Proceedings of the National Academy of Sciences*, 115(34):8505–8510, 2018.
- [17] Edward Nelson. Derivation of the Schrödinger equation from Newtonian mechanics. *Phys. Rev.*, 150:1079–1085, Oct 1966. doi: 10.1103/PhysRev.150.1079. URL <https://link.aps.org/doi/10.1103/PhysRev.150.1079>.
- [18] Francesco Guerra. Introduction to nelson stochastic mechanics as a model for quantum mechanics. *The Foundations of Quantum Mechanics—Historical Analysis and Open Questions: Lecce, 1993*, pages 339–355, 1995.
- [19] Edward Nelson. The mystery of stochastic mechanics. *Unpublished manuscript*, 2005.

- [20] Ling Yang, Zhilong Zhang, Yang Song, Shenda Hong, Runsheng Xu, Yue Zhao, Yingxia Shao, Wentao Zhang, Bin Cui, and Ming-Hsuan Yang. Diffusion models: A comprehensive survey of methods and applications. *arXiv preprint arXiv:2209.00796*, 2022.
- [21] Maurizio Serva. Relativistic stochastic processes associated to Klein-Gordon equation. In *Annales de l'IHP Physique théorique*, volume 49, pages 415–432, 1988.
- [22] Jussi Lindgren and Jukka Liukkonen. Quantum mechanics can be understood through stochastic optimization on spacetimes. *Scientific reports*, 9(1):19984, 2019.
- [23] Janus J Eriksen. Mean-field density matrix decompositions. *The Journal of Chemical Physics*, 153(21):214109, 2020.
- [24] Gonçalo dos Reis, Stefan Engelhardt, and Greig Smith. Simulation of mckean–vlasov sdes with super-linear growth. *IMA Journal of Numerical Analysis*, 42(1):874–922, 2022.
- [25] Joan Bruna, Benjamin Peherstorfer, and Eric Vanden-Eijnden. Neural galerkin scheme with active learning for high-dimensional evolution equations. *arXiv preprint arXiv:2203.01360*, 2022.
- [26] D. Pfau, J.S. Spencer, A.G. de G. Matthews, and W.M.C. Foulkes. Ab-initio solution of the many-electron Schrödinger equation with deep neural networks. *Phys. Rev. Research*, 2:033429, 2020. doi: 10.1103/PhysRevResearch.2.033429. URL <https://link.aps.org/doi/10.1103/PhysRevResearch.2.033429>.
- [27] Jan Hermann, Zeno Schätzle, and Frank Noé. Deep-neural-network solution of the electronic Schrödinger equation. *Nature Chemistry*, 12(10):891–897, 2020.
- [28] J. F. Corney and P. D. Drummond. Gaussian quantum Monte Carlo methods for fermions and bosons. *Physical Review Letters*, 93(26), dec 2004. doi: 10.1103/physrevlett.93.260401. URL <https://doi.org/10.1103/PhysRevLett.93.260401>.
- [29] John A Barker. A quantum-statistical Monte Carlo method; path integrals with boundary conditions. *The Journal of Chemical Physics*, 70(6):2914–2918, 1979.
- [30] Brian M Austin, Dmitry Yu Zubarev, and William A Lester Jr. Quantum Monte Carlo and related approaches. *Chemical reviews*, 112(1):263–288, 2012.
- [31] Tamar Schlick. *Molecular modeling and simulation: an interdisciplinary guide*, volume 2. Springer, 2010.
- [32] Jonathan Ho, Ajay Jain, and Pieter Abbeel. Denoising diffusion probabilistic models. *Advances in Neural Information Processing Systems*, 33:6840–6851, 2020.
- [33] K Andrew Cliffe, Mike B Giles, Robert Scheichl, and Aretha L Teckentrup. Multilevel Monte Carlo methods and applications to elliptic PDEs with random coefficients. *Computing and Visualization in Science*, 14:3–15, 2011.
- [34] Xavier Warin. Nesting Monte Carlo for high-dimensional non-linear PDEs. *Monte Carlo Methods and Applications*, 24(4):225–247, 2018.
- [35] Pierre Del Moral and Pierre Del Moral. *Feynman-Kac formulae*. Springer, 2004.
- [36] Jia-An Yan. From Feynman-Kac formula to Feynman integrals via analytic continuation. *Stochastic processes and their applications*, 54(2):215–232, 1994.
- [37] David Bohm. A suggested interpretation of the quantum theory in terms of "hidden" variables. I. *Phys. Rev.*, 85:166–179, Jan 1952. doi: 10.1103/PhysRev.85.166. URL <https://link.aps.org/doi/10.1103/PhysRev.85.166>.
- [38] Peter E Kloeden, Eckhard Platen, Peter E Kloeden, and Eckhard Platen. *Stochastic differential equations*. Springer, 1992.
- [39] Diederik P Kingma and Jimmy Ba. Adam: A method for stochastic optimization. *arXiv preprint arXiv:1412.6980*, 2014.

- [40] Arthur Jacot, Franck Gabriel, and Clément Hongler. Neural tangent kernel: Convergence and generalization in neural networks. *Advances in neural information processing systems*, 31, 2018.
- [41] Sifan Wang, Xinling Yu, and Paris Perdikaris. When and why PINNs fail to train: A neural tangent kernel perspective. *Journal of Computational Physics*, 449:110768, 2022.
- [42] Maxim Raginsky, Alexander Rakhlin, and Matus Telgarsky. Non-convex learning via stochastic gradient Langevin dynamics: a nonasymptotic analysis, 2017.
- [43] Boris Muzellec, Kanji Sato, Mathurin Massias, and Taiji Suzuki. Dimension-free convergence rates for gradient Langevin dynamics in RKHS, 2020.
- [44] Ethan Bernstein and Umesh Vazirani. Quantum complexity theory. *SIAM Journal on Computing*, 26(5):1411–1473, 1997. doi: 10.1137/S0097539796300921.
- [45] Peter W. Shor. Polynomial-time algorithms for prime factorization and discrete logarithms on a quantum computer. *SIAM Journal on Computing*, 26(5):1484–1509, oct 1997. doi: 10.1137/s0097539795293172. URL <https://doi.org/10.1137%2Fs0097539795293172>.
- [46] Daniel J Bernstein and Tanja Lange. Post-quantum cryptography. *Nature*, 549(7671):188–194, 2017.
- [47] Pauli Virtanen, Ralf Gommers, Travis E Oliphant, Matt Haberland, Tyler Reddy, David Cournapeau, Evgeni Burovski, Pearu Peterson, Warren Weckesser, Jonathan Bright, et al. Scipy 1.0: fundamental algorithms for scientific computing in python. *Nature methods*, 17(3):261–272, 2020.
- [48] Brian D.O. Anderson. Reverse-time diffusion equation models. *Stochastic Processes and their Applications*, 12(3):313–326, 1982.
- [49] Samuel Colin and Ward Struyve. Quantum non-equilibrium and relaxation to equilibrium for a class of de Broglie–Bohm-type theories. *New Journal of Physics*, 12(4):043008, 2010.
- [50] Nicholas M. Boffi and Eric Vanden-Eijnden. Probability flow solution of the Fokker-Planck equation, 2023.
- [51] Orlando Alvarez. String theory and holomorphic line bundles. In *7th Workshop on Grand Unification: ICOBAN 86*, 9 1986.
- [52] Carlos Tejero Prieto and Raffaele Vitolo. On the geometry of the energy operator in quantum mechanics. *International Journal of Geometric Methods in Modern Physics*, 11(07):1460027, aug 2014. doi: 10.1142/s0219887814600275. URL <https://doi.org/10.1142%2Fs0219887814600275>.
- [53] Timothy Wallstrom. On the derivation of the Schrödinger equation from stochastic mechanics. *Foundations of Physics Letters*, 2:113–126, 03 1989. doi: 10.1007/BF00696108.
- [54] J Peter May. *A concise course in algebraic topology*. University of Chicago press, 1999.
- [55] István Gyöngy. Mimicking the one-dimensional marginal distributions of processes having an Itô differential. *Probability theory and related fields*, 71(4):501–516, 1986.
- [56] RG Woolley and BT Sutcliffe. Molecular structure and the born—Oppenheimer approximation. *Chemical Physics Letters*, 45(2):393–398, 1977.
- [57] Maaneli Derakhshani and Guido Bacciagaluppi. On multi-time correlations in stochastic mechanics, 2022.
- [58] Gordon D Smith and Gordon D Smith. *Numerical solution of partial differential equations: finite difference methods*. Oxford university press, 1985.
- [59] Silvana Ilie, Kenneth R Jackson, and Wayne H Enright. Adaptive time-stepping for the strong numerical solution of stochastic differential equations. *Numerical Algorithms*, 68(4):791–812, 2015.

- [60] Ph Blanchard, Ph Combe, M Sirugue, and M Sirugue-Collin. Stochastic jump processes associated with Dirac equation. In *Stochastic Processes in Classical and Quantum Systems: Proceedings of the 1st Ascona-Como International Conference, Held in Ascona, Ticino (Switzerland), June 24–29, 1985*, pages 65–86. Springer, 2005.
- [61] Vladimir N Serkin and Akira Hasegawa. Novel soliton solutions of the nonlinear Schrödinger equation model. *Physical Review Letters*, 85(21):4502, 2000.
- [62] Rainer Buckdahn, Juan Li, Shige Peng, and Catherine Rainer. Mean-field stochastic differential equations and associated PDEs. *The Annals of Probability*, 45(2):824 – 878, 2017. doi: 10.1214/15-AOP1076. URL <https://doi.org/10.1214/15-AOP1076>.
- [63] Rainer Buckdahn, Juan Li, Shige Peng, and Catherine Rainer. Mean-field stochastic differential equations and associated PDEs. 2017.
- [64] Thaddeus George Dankel. Mechanics on manifolds and the incorporation of spin into nelson’s stochastic mechanics. *Archive for Rational Mechanics and Analysis*, 37:192–221, 1970.
- [65] GF De Angelis, A Rinaldi, and M Serva. Imaginary-time path integral for a relativistic spin-(1/2) particle in a magnetic field. *Europhysics Letters*, 14(2):95, 1991.

## A Notation

- $\langle a, b \rangle = \sum_{i=1}^d a_i b_i$  for  $a, b \in \mathbb{R}^d$  – a scalar product.
- $\|a\| = \sqrt{\langle a, a \rangle}$  for  $a \in \mathbb{R}^d$  – a norm.
- $\text{Tr}(A) = \sum_{i=1}^d a_{ii}$  for a matrix  $A = [a_{ij}]_{i=1,j=1}^{d,d}$ .
- $A(t), B(t), C(t), \dots$  – stochastic processes indexed by time  $t \geq 0$ .
- $A_i, B_i, C_i, \dots$  – approximations to those processes.
- $a, b, c$  – other variables.
- $\mathbf{A}, \mathbf{B}, \mathbf{C}, \dots$  – quantum observables, e.g.,  $\mathbf{X}(t)$  – result of quantum measurement of the coordinate of the particle at moment  $t$ .
- $\rho_A(x, t)$  – density probability of a process  $A(t)$  at time  $t$ .
- $\psi(x, t)$  – a wave function.
- $\psi_0 = \psi(x, 0)$  – an initial wave function.
- $\rho(x, t) = |\psi(x, t)|^2$  – a quantum density.
- $\rho_0(x) = \rho(x, 0)$  – an initial probability distribution.
- $\psi(x, t) = \sqrt{\rho(x, t)} e^{iS(x, t)}$  where  $S(x, t)$  – a single-valued representative of the phase of the wave function.
- $\nabla = \left( \frac{\partial}{\partial x_1}, \dots, \frac{\partial}{\partial x_d} \right)$  – a gradient operator. If  $f : \mathbb{R}^d \rightarrow \mathbb{R}^m$ , then  $\nabla f(x) \in \mathbb{R}^{d \times m}$  is the Jacobian of  $f$ , in the case of  $m = 1$  we call it a gradient of  $f$ .
- $\nabla^2 = \left[ \frac{\partial^2}{\partial x_i \partial x_j} \right]_{i=1,j=1}^{d,d}$  – the Hessian operator.
- $\nabla^2 \cdot A = \left[ \frac{\partial^2}{\partial x_i \partial x_j} a_{ij} \right]_{i=1,j=1}^{d,d}$  for  $A = [a_{ij}(x)]_{i=1,j=1}^{d,d}$ .
- $\langle \nabla, \cdot \rangle$  – a divergence operator, e.g., for  $f : \mathbb{R}^d \rightarrow \mathbb{R}^d$  we have  $\langle \nabla, f(x) \rangle = \sum_{i=1}^d \frac{\partial}{\partial x_i} f_i(x)$ .
- $\Delta = \text{Tr}(\nabla^2)$  – the Laplace operator.
- $m$  – a mass tensor (or a scalar mass).
- $\hbar$  – the reduced Planck's constant.
- $\partial_y = \frac{\partial}{\partial y}$  – a short-hand notation for a partial derivative operator.
- $[A, B] = AB - BA$  – a commutator of two operators. If one of the arguments is a scalar function, we consider a scalar function as a point-wise multiplication operator.
- $|z| = \sqrt{x^2 + y^2}$  for a complex number  $z = x + iy \in \mathbb{C}$ ,  $x, y \in \mathbb{R}$ .
- $\mathcal{N}(\mu, C)$  – a Gaussian distribution with mean  $\mu \in \mathbb{R}^d$  and covariance  $C \in \mathbb{R}^{d \times d}$ .
- $A \sim \rho$  means that  $A$  is a random variable with distribution  $\rho$ . We do not differentiate between "sample from" and "distributed as", but it is evident from context when we consider samples from distribution versus when we say that something has such distribution.
- $\delta_x$  – delta-distribution concentrated at  $x$ . It is a generalized function corresponding to the "density" of a distribution with a singular support  $\{x\}$ .



## B DSM algorithm

We present detailed versions of our method: Algorithm 2 for batch generation and Algorithm 3 for training. During inference, distributions of  $X_i$  converge to  $\rho = |\psi|^2$  and thus we obtain the desired outcome. Furthermore, solving (7a) on points generated by the current best approximations of  $u, v$ , the method exhibits self-adaptation behavior: the method obtains its current belief where  $X(t)$  is concentrated, updates its belief and iterates accordingly. With each iteration of the inference, the method focuses more on high-concentration regions of  $\rho$ .

---

**Algorithm 2** GenerateBatch( $u, v, \rho_0, \nu, T, B, N$ ) – sample trajectories

---

**Physical hyperparams:**  $T$  – time horizon,  $\psi_0$  – initial wave-function.

**Hyperparams:**  $\nu \geq 0$  – diffusion constant,  $B \geq 1$  – batch size,  $N \geq 1$  – time grid size.

$t_i = iT/N$  for  $0 \leq i \leq N$

sample  $X_{0j} \sim |\psi_0|^2$  for  $1 \leq jB$

**for**  $1 \leq i \leq N$  **do**

sample  $\xi_j \sim \mathcal{N}(0, I_d)$  for  $1 \leq j \leq B$

$X_{ij} = X_{(i-1)j} + \frac{T}{N}(v_\theta(X_{(i-1)j}, t_{i-1}) + \nu u_\theta(X_{(i-1)j}, t_{i-1})) + \sqrt{\frac{\nu \hbar T}{mN}} \xi_j$  for  $1 \leq j \leq B$

**end for**

**output**  $\left\{ \{X_{ij}\}_{j=1}^B \right\}_{i=0}^N$

---



---

**Algorithm 3** A training algorithm

---

**Physical hyperparams:**  $m > 0$  – mass,  $\hbar > 0$  – reduced Planck constant,  $T$  – a time horizon,  $\psi_0 : \mathbb{R}^d \rightarrow \mathbb{C}$  – an initial wave function,  $V : \mathbb{R}^d \times [0, T] \rightarrow \mathbb{R}$  – potential.

**Hyperparams:**  $\eta > 0$  – learning rate for backprop,  $\nu > 0$  – diffusion constant,  $B \geq 1$  – batch size,  $M \geq 1$  – optimization steps,  $N \geq 1$  – time grid size,  $w_u, w_v, w_0 > 0$  – weights of losses.

**Instructions:**

$t_i = iT/N$  for  $0 \leq i \leq N$

**for**  $1 \leq \tau \leq M$  **do**

$X = \text{GenerateBatch}(u_{\theta_{\tau-1}}, v_{\theta_{\tau-1}}, \psi_0, \nu, T, B, N)$

define  $L_\tau^u(\theta) = \frac{1}{(N+1)B} \sum_{i=0}^N \sum_{j=1}^B \|\partial_t u_\theta(X_{ij}, t_i) - \mathcal{D}_u[u_\theta, v_\theta, X_{ij}, t_i]\|^2$

define  $L_\tau^v(\theta) = \frac{1}{(N+1)B} \sum_{i=0}^N \sum_{j=1}^B \|\partial_t v_\theta(X_{ij}, t_i) - \mathcal{D}_v[u_\theta, v_\theta, X_{ij}, t_i]\|^2$

define  $L_\tau^0(\theta) = \frac{1}{B} \sum_{j=1}^B \left( \|u_\theta(X_{0j}, t_0) - u_0(X_{0j}, t_0)\|^2 + \|v_\theta(X_{0j}, t_0) - v_0(X_{0j}, t_0)\|^2 \right)$

define  $\mathcal{L}_\tau(\theta) = w_u L_\tau^u(\theta) + w_v L_\tau^v(\theta) + w_0 L_\tau^0(\theta)$

$\theta_\tau = \text{OptimizationStep}(\theta_{\tau-1}, \nabla_\theta \mathcal{L}_\tau(\theta_{\tau-1}), \eta)$

**end for**

**output**  $u_{\theta_M}, v_{\theta_M}$

---

## C Experimental setup details

In our experiments, we set  $m = 1$ ,  $\hbar = 10^{-25}$ ,  $\sigma^2 = 10^{-1}$ . For the harmonic oscillator model,  $N = 1000$  and the batch size  $B = 100$ ; for the singular initial condition problem,  $N = 100$  and  $B = 100$ . For evaluation, our method samples 10 000 points per time step, and the observables are estimated from these samples; we run the model this way ten times.

### C.1 A numerical solution

**1d harmonic oscillator with  $S_0(x) \equiv 0$ :** To evaluate our method’s performance, we use a numerical solver that integrates the corresponding differential equation given the initial condition. We use SciPy library [47]. The solution domain is  $x \in [-2, 2]$  and  $t \in [0, 1]$ , where  $x$  is split into 566 points and  $t$

---

<sup>5</sup>The value of the reduced Plank constant depends on the metric system that we use and, thus, for our evaluations we are free to choose any value.

into 1001 time steps. This solution can be repeated  $d$  times for the  $d$ -dimensional harmonic oscillator problem.

**1d harmonic oscillator with  $S_0(x) = -5x$ :** We use the same numerical solver as for the  $S_0(x) \equiv 0$  case. The solution domain is  $x \in [-2, 2]$  and  $t \in [0, 1]$ , where  $x$  is split into 2829 points and  $t$  is split into 1001 time steps.

## C.2 Architecture and training details

A basic NN architecture for our approach and the PINN is a feed-forward NN with one hidden layer with hyperbolic tangent activation functions. We represent the velocities  $u$  and  $v$  using the basic NN architecture with 200 neurons in the case of the singular initial condition. The training process takes about 7 mins. For  $d = 1$  harmonic oscillator with zero initial phase problem, there are 200 neurons for our method and 400 for the PINN; for  $d = 3$  and more dimensions, we use 400 neurons. This rule holds for the experiments measuring total training time in Section 6. In a  $d = 1$  harmonic oscillator with a non-zero initial phase problem, we use 300 hidden neurons in our models. In the experiments devoted to measuring time per epoch, the number of hidden neurons is fixed to 200 for all dimensions. We use Adam optimizer [39] with a learning rate  $10^{-4}$ . In our experiments, we set  $w_u = 1, w_v = 0.8, w_0 = 1$ . For PINN evaluation, the test sets are the same as the grid for the numerical solver. In our experiments, we usually use a single NVIDIA A40 GPU. For the results reported in Section 6.3, we use an NVIDIA A100 GPU.

## D Results

### D.1 3d harmonic oscillator

Here, we provide results for a 3d harmonic oscillator. Figure 5 demonstrates the obtained statistics with the proposed algorithm's two versions (Nelsonian and Gradient Divergence) for every dimension. Figure 6 compares the density function for every dimension for these two versions. Table 3 summarizes the error rates per dimension. The results suggest no significant difference in the performance of these two versions of our algorithm. As mentioned in the main text, the Gradient Divergence version tends to require more steps to converge, but it has linear time complexity in contrast to the quadratic complexity of the Nelsonian version.

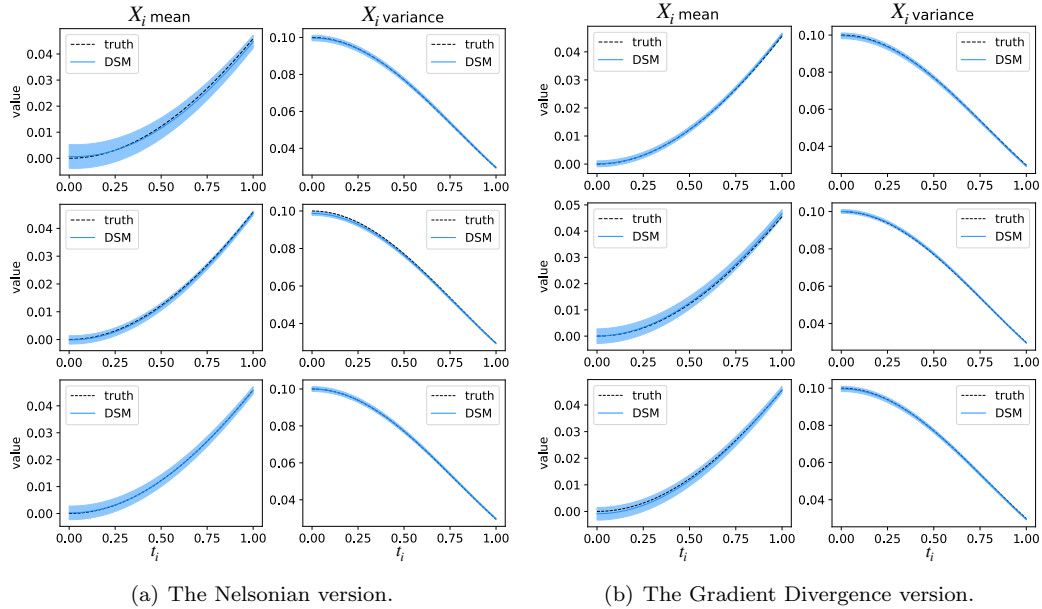


Figure 5: The obtained statistics for 3d harmonic oscillator using two versions of the proposed approach.

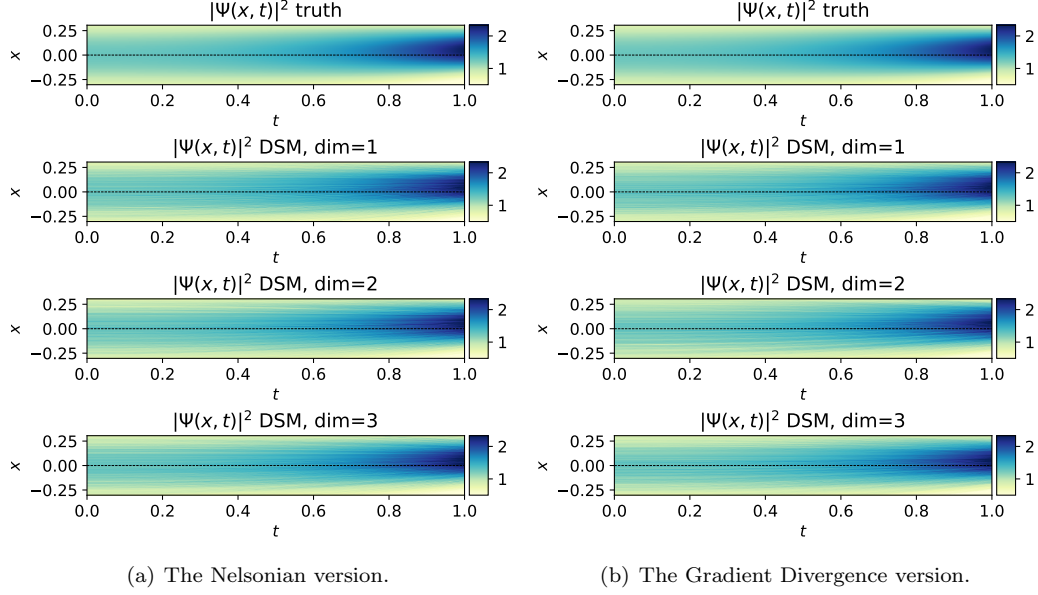


Figure 6: The density function for 3d harmonic oscillator using two versions of the proposed approach.

Table 3: The results for 3d harmonic oscillator with  $S_0(x) \equiv 0$  using two versions of the proposed approach: the Nelsonian one uses the Laplacian operator in the training loss, the Gradient Divergence version is our modification that replaces Laplacian with gradient of divergence.

Model	$\mathcal{E}_m(X_i^{(1)}) \downarrow$	$\mathcal{E}_m(X_i^{(2)}) \downarrow$	$\mathcal{E}_m(X_i^{(3)}) \downarrow$	$\mathcal{E}_m(X_i) \downarrow$
DSM (Nelsonian)	$0.170 \pm 0.081$	$0.056 \pm 0.030$	<b><math>0.073 \pm 0.072</math></b>	$0.100 \pm 0.061$
DSM (Gradient Divergence)	<b><math>0.038 \pm 0.023</math></b>	<b><math>0.100 \pm 0.060</math></b>	$0.082 \pm 0.060$	<b><math>0.073 \pm 0.048</math></b>
Model	$\mathcal{E}_v(X_i^{(1)}) \downarrow$	$\mathcal{E}_v(X_i^{(2)}) \downarrow$	$\mathcal{E}_v(X_i^{(3)}) \downarrow$	$\mathcal{E}_v(X_i) \downarrow$
DSM (Nelsonian)	<b><math>0.012 \pm 0.009</math></b>	$0.012 \pm 0.009$	$0.011 \pm 0.008$	$0.012 \pm 0.009$
DSM (Gradient Divergence)	<b><math>0.012 \pm 0.010</math></b>	<b><math>0.009 \pm 0.005</math></b>	<b><math>0.011 \pm 0.010</math></b>	<b><math>0.011 \pm 0.008</math></b>
Model	$\mathcal{E}(v^{(1)}) \downarrow$	$\mathcal{E}(v^{(2)}) \downarrow$	$\mathcal{E}(v^{(3)}) \downarrow$	$\mathcal{E}(v) \downarrow$
DSM (Nelsonian)	0.00013	0.00012	0.00012	0.00012
DSM (Gradient Divergence)	<b><math>4.346 \times 10^{-5}</math></b>	<b><math>4.401 \times 10^{-5}</math></b>	<b><math>4.700 \times 10^{-5}</math></b>	<b><math>4.482 \times 10^{-5}</math></b>
Model	$\mathcal{E}(u^{(1)}) \downarrow$	$\mathcal{E}(v^{(2)}) \downarrow$	$\mathcal{E}(v^{(3)}) \downarrow$	$\mathcal{E}(v) \downarrow$
DSM (Nelsonian)	<b><math>4.441 \times 10^{-5}</math></b>	<b><math>2.721 \times 10^{-5}</math></b>	$2.810 \times 10^{-5}$	<b><math>3.324 \times 10^{-5}</math></b>
DSM (Gradient Divergence)	$6.648 \times 10^{-5}$	$4.405 \times 10^{-5}$	<b><math>1.915 \times 10^{-5}</math></b>	$4.333 \times 10^{-5}$

## D.2 Computational complexity

We empirically estimate memory allocation on a GPU (NVIDIA A100) when training two versions of the proposed algorithm. In addition, we estimate the number of epochs until the training loss function is less than  $10^{-2}$  for different problem dimensions. The results are visualized in Figure 7(a) proves the memory usage of the Gradient Divergence version grows linearly with the dimension while it grows quadratically in the Nelsonian version. We also empirically access the convergence speed of two versions of our approach. Figure 7(b) shows how many epochs are needed to make the training loss less than  $1 \times 10^{-2}$ . Usually, the Gradient Divergence version requires slightly more epochs to converge to this threshold than the Nelsonian one. The number of epochs is averaged across five runs. In both experiments, the setup is the same as we describe in Section 6.3.

Also, we provide more details on the experiment measuring the total training time per dimensions  $d = 1, 3, 5, 7, 9$ . This experiment is described in Section 6.3, and the training time grows linearly with the problem dimension. Table 4 presents the error rates and train time. The results show that the

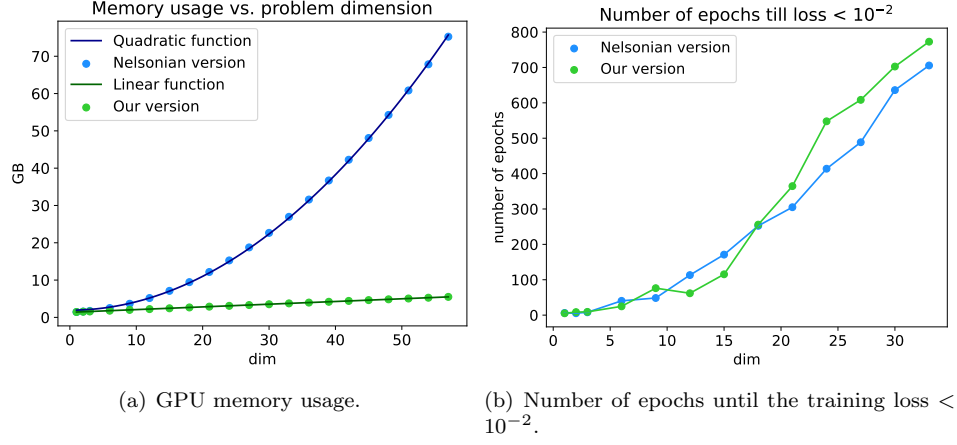


Figure 7: Empirical complexity evaluation of two versions of the proposed method: memory usage and the number of epochs until the loss is less than the threshold.

proposed approach can perform well for every dimension while the train time scales linearly with the problem dimension.

Table 4: Training time and test errors for the harmonic oscillator model for different  $d$ .

$d$	$\mathcal{E}_m(X_i) \downarrow$	$\mathcal{E}_v(X_i) \downarrow$	$\mathcal{E}(v) \downarrow$	$\mathcal{E}(u) \downarrow$	Train time
1	$0.074 \pm 0.052$	$0.009 \pm 0.007$	0.00012	2.809e-05	46m 20s
3	$0.073 \pm 0.048$	$0.010 \pm 0.008$	4.479e-05	3.946e-05	2h 18m
5	$0.081 \pm 0.057$	$0.009 \pm 0.008$	4.956e-05	4.000e-05	3h 10m
7	$0.085 \pm 0.060$	$0.011 \pm 0.009$	5.877e-05	4.971e-05	3h 40m
9	$0.096 \pm 0.081$	$0.011 \pm 0.009$	7.011e-05	6.123e-05	4h 46m

## E Stochastic Processes for Quantum Mechanics

### E.1 Diffusion processes

We consider the Ito diffusion processes:

$$dX(t) = b(X(t), t)dt + \sigma(X(t), t)dW(t), \quad (16)$$

$$X(0) \sim \rho_0, \quad (17)$$

where  $W(t) \in \mathbb{R}^d$  is the standard Wiener process,  $b : \mathbb{R}^d \times [0, T] \rightarrow \mathbb{R}^d$  is the drift function, and  $\sigma : \mathbb{R}^d \times [0, T] \rightarrow \mathbb{R}^{d \times d}$  is a symmetric positive definite matrix-valued function called a diffusion coefficient. Essentially,  $X(t)$  samples from  $\rho_X = \text{Law}(X(t))$  for each  $t \in [0, T]$ . Thus, we may wonder how to define  $b$  and  $\sigma$  to ensure  $\rho_X = |\psi|^2$ .

There is the forward Kolmogorov equation for the density  $\rho_X$  associated with this diffusion process:

$$\partial_t \rho_X = \langle \nabla, b \rho_X \rangle + \frac{1}{2} \text{Tr}(\nabla^2 \cdot (\sigma \sigma^T \rho_X)). \quad (18)$$

Moreover, the diffusion process is time reversible. This leads to the backward Kolmogorov equation:

$$\partial_t \rho_X = \langle \nabla, b^* \rho_X \rangle - \frac{1}{2} \text{Tr}(\nabla^2 \cdot (\sigma \sigma^T \rho_X)), \quad (19)$$

where  $b_i^* = b_i - \rho_X^{-1} \langle \nabla, \sigma \sigma^T e_i \rho_X \rangle$  with  $e_{ij} = \delta_{ij}$  for  $j \in \{1, \dots, d\}$ . Summing up those two equations, we obtain the following:

$$\partial_t \rho_X = \langle \nabla, v \rho_X \rangle, \quad (20)$$

where  $v = \frac{b+b^*}{2}$  is so called probability current. This is the continuity equation for the Ito diffusion process Equation (16). We refer to [48] for details. We note that the same (20) can be obtained with arbitrary non-singular  $\sigma(x, t)$  as long as  $v = v(x, t)$  remains fixed.

## E.2 From Schrödinger to Continuity

Let's consider the Schrödinger equation:

$$i\hbar\partial_t\psi = \left(-\frac{\hbar^2}{2m}\Delta + V\right)\psi, \quad (21)$$

$$\psi(\cdot, 0) = \psi_0 \quad (22)$$

where  $\Delta = \text{Tr}(\nabla^2) = \sum_{i=1}^d \frac{\partial^2}{\partial x_i^2}$  is the Laplace operator. The second cohomology is trivial in this case. So, we can assume that  $\psi = \sqrt{\rho}e^{iS}$  with  $S(x, t)$  is a single-valued function.

By defining the drift  $v = \frac{\hbar}{m}\nabla S$ , we can derive quantum mechanics continuity equation on density  $\rho$ :

$$\partial_t\rho = \langle \nabla, v\rho \rangle, \quad (23)$$

$$\rho(\cdot, 0) = |\psi_0|^2. \quad (24)$$

This immediately tells us what should be initial distribution  $\rho_0$  and  $\frac{b+b^*}{2}$  for the Ito diffusion process (16).

## E.3 From Continuity to Kolmogorov

For now, the only missing parts for obtaining the diffusion process from the quantum mechanics continuity equation are to identify the term  $\frac{b-b^*}{2}$  and the diffusion coefficient  $\sigma$ . Both of them should be related as  $(b-b^*)_i = \rho^{-1}\langle \nabla, \sigma\sigma^T e_i\rho \rangle$ . Thus, we can pick  $\sigma \propto I_d$  to simplify the equations. Nevertheless, our results can be extended to any non-trivial diffusion coefficient. Therefore, by defining  $u(x, t) = \frac{\hbar}{2m}\nabla \log \rho(x, t)$  and using arbitrary  $\nu > 0$  we derive

$$\partial_t\rho = \langle \nabla, (v + \nu u)\rho \rangle + \frac{\nu\hbar}{2m}\Delta\rho. \quad (25)$$

Thus, we can sample from  $\rho_X(x, t) \equiv \rho(x, t)$  using the diffusion process with  $b(x, t) = v(x, t) + \nu u(x, t)$  and  $\sigma(x, t) \equiv \frac{\nu\hbar}{m}I_d$ :

$$dX(t) = (v(X(t), t) + \nu u(X(t), t))dt + \sqrt{\frac{\nu\hbar}{m}}dW(t), \quad (26)$$

$$X(0) \sim |\psi_0|^2. \quad (27)$$

To obtain numerical samples from the diffusion, one can use any numerical integrator, for example, the Euler-Maryama integrator [38]:

$$X_{i+1} = X_i + (v(X_i, t_i) + \nu u(X_i, t_i))\epsilon + \sqrt{\frac{\nu\hbar}{m}}\epsilon\mathcal{N}(0, I_d), \quad (28)$$

$$X_0 \sim |\psi_0|^2, \quad (29)$$

where  $\epsilon > 0$  is a step size,  $0 \leq i < \frac{T}{\epsilon}$ . We consider this type of integrator in our work. However, integrators of higher order, e.g., Runge-Kutta family of integrators [38], can achieve the same integration error with larger  $\epsilon > 0$ ; this approach is out of the scope of our work.

For cases of  $|\psi_0|^2 > 0$  everywhere, e.g., if the initial conditions are gaussian but not singular like  $\delta_{x_0}$ , we can actually set  $\nu = 0$  to obtain deterministic flow:

$$dX(t) = v(X(t), t)dt, \quad (30)$$

$$X(0) \sim |\psi_0|^2 \quad (31)$$

This is the guiding equation in Bohr's pilot-wave theory [37]. The major drawback of using Bohr's interpretation is that  $\rho_X$  may not equal  $\rho = |\psi|^2$ , a phenomenon known as quantum non-equilibrium [49]. Though, under certain mild conditions [50] (one of which is  $|\psi_0|^2 > 0$  everywhere) time marginals of such deterministic process  $X(t)$  will satisfy  $\text{Law}(X(t)) = \rho$  for each  $t \in [0, T]$ . As with the SDE case, it is unlikely that those trajectories are "true" trajectories. It only matters that their time marginals coincide with true quantum mechanical densities.

## F Stochastic Mechanics Derivation

Let's consider the polar decomposition once again  $\psi = \sqrt{\rho}e^{iS}$ . Observe for  $\partial \in \{\partial_t, \partial_{x_i}\}$  that:

$$\begin{aligned}\partial\psi &= (\partial\sqrt{\rho})e^{iS} + (i\partial S)\psi = \frac{\partial\rho}{2\sqrt{\rho}}e^{iS} + (i\partial S)\psi = \frac{1}{2}\frac{\partial\rho}{\rho}\sqrt{\rho}e^{iS} + (i\partial S)\psi = \left(\frac{1}{2}\partial\log\rho + i\partial S\right)\psi, \\ \partial^2\psi &= \partial\left(\left(\frac{1}{2}\partial\log\rho + i\partial S\right)\psi\right) = \left(\frac{1}{2}\partial^2\log\rho + i\partial^2S + \left(\frac{1}{2}\partial\log\rho + i\partial S\right)^2\right)\psi\end{aligned}$$

Substituting it into the Schrödinger equation:

$$i\hbar\left(\frac{1}{2}\partial_t\log\rho + i\partial_tS\right)\psi = -\frac{\hbar^2}{2m}\left(\frac{1}{2}\Delta\log\rho + i\Delta S + \left\|\frac{1}{2}\nabla\log\rho + i\nabla S\right\|^2\right)\psi + V\psi \quad (32)$$

Dividing by  $\psi^6$  and separating real and imaginary parts, we obtain:

$$-\hbar\partial_tS = -\frac{\hbar^2}{2m}\left(\frac{1}{2}\Delta\log\rho + \frac{1}{4}\|\log\rho\|^2 - \|\nabla S\|^2\right) + V, \quad (33)$$

$$\frac{\hbar}{2}\partial_t\log\rho = -\frac{\hbar^2}{2m}(\Delta S + \langle\log\rho, \nabla S\rangle). \quad (34)$$

Noting that  $\Delta = \langle\nabla, \nabla\cdot\rangle$  and substituting  $v = \frac{\hbar}{m}\nabla S, u = \frac{\hbar}{2m}\log\rho$  to simplify we obtain:

$$m\frac{\hbar}{m}\partial_tS = \frac{\hbar}{2m}\langle\nabla, u\rangle + \frac{1}{2}\|u\|^2 - \frac{1}{2}\|v\|^2 - V, \quad (35)$$

$$\frac{\hbar}{2m}\partial_t\log\rho = -\frac{\hbar}{2m}\langle\nabla, v\rangle - \langle u, v\rangle. \quad (36)$$

Finally, by taking  $\nabla$  from both parts, noting that  $[\nabla, \partial_t] = 0$  for scalar functions and again substituting  $u, v$ , we arrive at:

$$\partial_tv = -\frac{1}{m}\nabla V + \langle u, \nabla\rangle u - \langle v, \nabla\rangle v + \frac{\hbar}{2m}\nabla\langle\nabla, u\rangle \quad (37)$$

$$\partial_tu = -\nabla\langle v, u\rangle - \frac{\hbar}{2m}\nabla\langle\nabla, v\rangle. \quad (38)$$

To get the initial conditions on the velocities of the process  $v_0 = v(x, 0)$  and  $u_0 = u(x, 0)$ , we can refer to the equations that we used in the derivation

$$v(x, t) = \frac{\hbar}{m}\nabla S(x, t), \quad (39)$$

$$u(x, t) = \frac{\hbar}{2m}\nabla\log\rho(x, t) \quad (40)$$

Substituting  $t = 0$  we can get our initial conditions on  $v_0(x) = \frac{\hbar}{m}\nabla S(x, 0), u_0(x) = \frac{\hbar}{2m}\nabla\log\rho_0(x)$  where  $\rho_0(x) = \rho(x, 0)$ .

For more detailed derivation and proof of equivalence of those two equations to the Schrödinger one, see [17, 19, 18]. Moreover, this equivalence holds for manifolds  $\mathcal{M}$  with trivial second cohomology group as noted in [51, 52, 53].

---

<sup>6</sup>Here, we assume  $\psi \neq 0$ . Even though it may seem a restriction, in our method, we will solve equations only on  $X(t)$  which satisfy  $\mathbb{P}(\psi(X(t), t) = 0) = 0$ , thus, we are allowed to assume this safely without loss of generality. The same cannot be said if we considered the PINN over a grid to solve our equations.

## F.1 Equations of Stochastic Mechanics

We note that our equations differ from [17, 18]. In [17], we see

$$\partial_t v = -\frac{1}{m}\nabla V + \langle u, \nabla \rangle u - \langle v, \nabla \rangle v + \frac{\hbar}{2m}\Delta u, \quad (41)$$

$$\partial_t u = -\nabla \langle v, u \rangle - \frac{\hbar}{2m}\nabla \langle \nabla, v \rangle; \quad (42)$$

and in [18], we see

$$\partial_t v = -\frac{1}{m}\nabla V + \langle u, \nabla \rangle u - \langle v, \nabla \rangle v + \frac{\hbar}{2m}\Delta u, \quad (43)$$

$$\partial_t u = -\nabla \langle v, u \rangle - \frac{\hbar}{2m}\Delta v. \quad (44)$$

The discrepancy seems to occur because the work [19] covers the case of the multi-valued  $S$  and thus does not assume that  $[\Delta, \nabla] = 0$  to transform  $\nabla \langle \nabla, \nabla S \rangle$  into  $\Delta(\nabla S)$  to make the equations work for the case of a non-trivial cohomology group of  $\mathcal{M}$ . So, [19] does not transform  $\nabla \langle \nabla, \nabla S \rangle$  into  $\Delta(\nabla S)$ , but [18] uses  $\Delta(\nabla S)$ . Computing  $\Delta$  with autograd tools requires  $\mathcal{O}(d^2)$  operations as it requires computing the full Hessian  $\nabla^2$ . Instead, we treat  $\log \rho$  as it can be multi-valued not because we want more generality but because we want to have  $\mathcal{O}(d)$  computational time in the dimension as computing  $\nabla \langle \nabla, \cdot \rangle$  is much easier with autograd tools. Generally, we cannot swap  $\Delta$  with  $\nabla \langle \nabla, \cdot \rangle$  unless the solutions of the equation can be represented as full gradients of some function, which is the case for stochastic mechanical equations but not for the Shrödinger one. For some reason, it is not discussed in [19, 17, 18], but it is the reason why the equations in [17, 18] are different.

We derive equations different from both works and provide insights into why there are four different equivalent sets of equations (by changing  $\Delta$  with  $\nabla \langle \nabla, \cdot \rangle$  in both equations independently). From a numerical perspective, it is more beneficial to avoid Laplacian calculations. However, we notice that inference using equations from [17] converges faster by iterations to the true  $u, v$  compared to our version. It comes at the cost of a severe slowdown in each iteration for  $d \gg 1$ , which diminishes the benefit since the overall training time to get comparable results decreases significantly.

## F.2 Interpolation between Bohmian and Nelsonian pictures

We also differ from [17] since we define  $u$  without  $\nu$ . We bring it into the picture separately as a multiplicative factor:

$$dX(t) = (v(X(t), t) + \nu u(X(t), t))dt + \sqrt{\frac{\nu \hbar}{m}}dW(t), \quad (45)$$

$$X(0) \sim |\psi_0|^2 \quad (46)$$

This trick allows us to recover Nelson's diffusion when  $\nu = 1$ :

$$dX(t) = (v(X(t), t) + u(X(t), t))dt + \sqrt{\frac{\hbar}{m}}dW(t), \quad (47)$$

$$X(0) \sim |\psi_0|^2 \quad (48)$$

And, moreover, for  $\nu = 0$  we recover the deterministic pilot-wave theory [37]:

$$dX(t) = v(X(t), t)dt, \quad (49)$$

$$X(0) \sim |\psi_0|^2. \quad (50)$$

We remind that  $\nu = 0$  case is valid only under certain regularity conditions on  $|\psi_0|^2$  [50], e.g.,  $|\psi_0|^2 > 0$  everywhere, otherwise we may have non-equilibrium case [49] which renders  $X(t)$  not being distributed as  $|\psi|^2$ . Thus, applications of  $\nu = 0$  should be careful, and if you are unsure that it can be used in your particular case, then use  $\nu = 1$  to avoid mistakes.



## G On criticism of Stochastic Mechanics

Three major concerns arise regarding stochastic mechanics developed by [17, 18]:

- The proof of the equivalence of stochastic mechanics to classic quantum mechanics relies on an implicit assumption of the phase  $S(x, t)$  being single-valued [53].
- If there is an underlying stochastic process of quantum mechanics, it should be non-Markovian [19].
- For a quantum observable, e.g., a position operator  $\mathbf{X}(t)$ , a compound distribution of positions at two different timestamps  $t, t'$  does not match distribution of  $(\mathbf{X}(t), \mathbf{X}(t'))$  [19].

Appendix H.4 discusses why a mismatch of the distributions is not a problem and how we can adopt stochastic mechanics with our approach to get correct compound distributions by incorporating the measurement process into the stochastic mechanical picture.

### G.1 On “inequivalence” to Schrödinger equation

This problem is explored in the paper [53]. Firstly, the authors argue that proofs of the equivalency in [17, 18] are based on the assumption that the wave function phase  $S$  is single-valued. In the general case of a multi-valued phase, the wave functions are identified with sections of complex line bundles over  $\mathcal{M}$ . In the case of a trivial line bundle, the space of sections can be formed from single-valued functions, see [51]. The equivalence class of line bundles over a manifold  $\mathcal{M}$  is called Picard group, and for smooth manifolds,  $\mathcal{M}$  is isomorphic to  $H^2(\mathcal{M}, \mathbb{Z})$ , so-called second cohomology group over  $\mathbb{Z}$ , see [52] for details. Elements in this group give rise to non-equivalent quantizations with irremovable gauge symmetry phase factor.

Therefore, *in this paper, we assume that  $H^2(\mathcal{M}, \mathbb{Z}) = 0$* , which allows us to eliminate all criticism about non-equivalence. Under this assumption, stochastic mechanics is *equivalent* indeed. This condition holds when  $\mathcal{M} = \mathbb{R}^d$ . Though, if a potential  $V$  has singularities, e.g.,  $\frac{a}{\|x - x_*\|}$ , then we should exclude  $x_*$  from  $\mathbb{R}^d$  which leads to  $\mathcal{M} = \mathbb{R}^d \setminus \{x_*\}$  and this manifold satisfies  $H^2(\mathcal{M}, \mathbb{Z}) \cong \mathbb{Z}$  [54] which essentially leads to “counterexample” provided in [53]. We suggest a solution to this issue in Appendix H.2.

### G.2 On “superluminal” propagation of signals

We want to clarify why this work should not be judged from perspectives of *physical realism, correspondence to reality* and *interpretations* of quantum mechanics. This tool gives the exact predictions as classical quantum mechanics at a moment of measurement. Thus, we do not care about a superluminal change in the drifts of entangled particles and other problems of the Markovian version of stochastic mechanics.

### G.3 Non-Markovianity

Nelson believes [19] that an underlying stochastic process of reality should be non-Markovian to avoid issues with the Markovian processes like superluminal propagation of signals. Even if such a process were proposed in the future, it would not affect our approach. In stochastic calculus, there is a beautiful theorem from [55]:

**Theorem 1.** *Assume  $X(t), F(t), G(t)$  are adapted to Wiener process  $W(t)$  and satisfy:*

$$dX(t) = F(t)dt + G(t)dW(t).$$

*Then there exist a Markovian process  $Y(t)$  satisfying*

$$dY(t) = f(Y(t), t)dt + g(Y(t), t)dW(t)$$

*where  $f(x, t) = \mathbb{E}(F(t) | X(t) = x), g(x, t) = \sqrt{\mathbb{E}(G(t)G(t)^T | X(t) = x)}$  and such that  $\forall t$  holds  $\text{Law}(X(t)) = \text{Law}(Y(t))$ .*

This theorem tells us that we already know how to build a process  $Y(t)$  without knowing  $X(t)$ ; it is stochastic mechanics by Nelson [17, 18] that we know. From a numerical perspective, we better stick with  $Y(t)$  as it is easier to simulate, and as we explained, we do not care about correspondence to reality as long as it gives the same final results.

## H Applications

### H.1 Bounded domain $\mathcal{M}$

Our approach assumes that the manifold  $\mathcal{M}$  is flat or curved. For bounded domains  $\mathcal{M}$ , e.g., like it is assumed in PINN or any other grid-based methods, our approach can be applied if we embed  $\mathcal{M} \subset \mathbb{R}^d$  and define a new family of smooth non-singular potentials  $V_\alpha$  on entire  $\mathbb{R}^d$  such that  $V_\alpha \rightarrow V$  when restricted to  $\mathcal{M}$  and  $V_\alpha \rightarrow +\infty$  on  $\partial(\mathcal{M}, \mathbb{R}^d)$  (boundary of the manifold in embedded space) as  $\alpha \rightarrow 0_+$ .

### H.2 Singular initial conditions

It is possible to apply Algorithm 1 to  $\psi_0 = \delta_{x_0} e^{iS_0(x)}$  for some  $x_0 \in \mathcal{M}$ . We need to augment the initial conditions with a parameter  $\alpha > 0$  as  $\psi_0 = \sqrt{\frac{1}{\sqrt{2\pi\alpha^2}}} e^{-\frac{(x-x_0)^2}{2\alpha^2}}$  for small enough  $\alpha > 0$ . In that case,  $u_0(x) = -\frac{\hbar}{2m} \frac{(x-x_0)}{\alpha}$ . We must be careful with choosing  $\alpha$  to avoid numerical instability. It makes sense to try  $\alpha \propto \frac{\hbar^2}{m^2}$  as  $\frac{X(0)-x_0}{\alpha} = \mathcal{O}(\sqrt{\alpha})$ . We evaluated such a setup in Section 6.1.

### H.3 Singular potential

We must augment the potential to apply our method for simulations of the atomic nucleus with Bohr-Oppenheimer approximation [56]. A potential arising in this case has components of form  $\frac{a_{ij}}{\|x_i - x_j\|}$ . Basically, it has singularities when  $x_i = x_j$ . In case when  $x_j$  is fixed, our manifold is  $\mathcal{M} \setminus \{x_j\}$ , which has a non-trivial cohomology group.

When such potential arises we suggest to augment the potential  $V_\alpha$  (e.g., replace all  $\frac{a_{ij}}{\|x_i - x_j\|}$  with  $\frac{a_{ij}}{\sqrt{\|x_i - x_j\|^2 + \alpha}}$ ) so that  $V_\alpha$  is smooth and non-singular everywhere on  $\mathcal{M}$ . In that case we have that  $V_\alpha \rightarrow V$  as  $\alpha \rightarrow 0$ . With the augmented potential  $V_\alpha$ , we can apply stochastic mechanics to obtain an equivalent to quantum mechanics theory. Of course, augmentation will produce bias, but it will be asymptotically negligent as  $\alpha \rightarrow 0$ .

### H.4 Measurement

Even though we have entire trajectories and know positions for each moment, we should carefully interpret them. This is because they are not the result of the measurement process. Instead, they represent hidden variables (and  $u, v$  represent global hidden variables – what saves us from the Bells inequalities as stochastic mechanics is non-local [17]).

For a fixed  $t \in [0, T]$ , the distribution of  $X(t)$  coincides with the distribution  $\mathbf{X}(t)$  for  $\mathbf{X}$  being position operator in quantum mechanics. Unfortunately, a compound distribution  $(X(t), X(t'))$  for  $t \neq t'$  may not correspond to the compound distribution of  $(\mathbf{X}(t), \mathbf{X}(t'))$ ; for details see [19]. This is because each  $\mathbf{X}(t)$  is a result of the *measurement process*, which causes the wave function to collapse [57].

Trajectories  $X_i$  are as if we could measure  $\mathbf{X}(t)$  without causing the collapse of the wave function. To use this approach for predicting some experimental results involving multiple measurements, we need to re-run our method after each measurement process with the measured state as the new initial condition. This issue is not novel for stochastic mechanics. There is the same problem in classical quantum mechanics.

This “contradiction” is resolved once we realize that  $\mathbf{X}(t)$  involves measurement, and thus, if we want to calculate correlations of  $(\mathbf{X}(t), \mathbf{X}(t'))$  for  $t < t'$  we need to do the following:

- Run Algorithm 1 with  $\psi_0, V(x, t)$  and  $T = t$  to get  $\tilde{u}, \tilde{v}$ .

- Run Algorithm 2 with  $\tilde{u}, \tilde{v}, \psi_0$  to get  $\{X_{Nj}\}_{j=1}^B - B$  last steps from trajectories  $X_i$  of length  $N$ .
- For each  $X_{Nj}$  in the batch we need to run Algorithm 1 with  $\psi_0 = \delta_{X_{Nj}}, V'(x, t') = V(x, t' + t)$  (assuming that  $u_0 = 0, v_0 = 0$ ) and  $T = t' - t$  to get  $\tilde{u}_j, \tilde{v}_j$ .
- For each  $X_{Nj}$  run Algorithm 2 with batch size  $B = 1, \psi_0 = \delta_{X_{Nj}}, \tilde{u}_j, \tilde{v}_j$  to get  $X'_{Nj}$ .
- Output pairs  $\{(X_{N,j}, X'_{N,j})\}_{j=1}^B$ .

Then the distribution of  $(X_{N,j}, X'_{N,j})$  will correspond to the distribution of  $(\mathbf{X}(t), \mathbf{X}(t'))$ . This is well described and proven in [57]. Therefore, it is possible to simulate the right correlations in time using our approach, though, it may require learning  $2(B + 1)$  models. The promising direction of future research is to consider  $X_0$  as a feature for the third step here and, thus, learn only  $2 + 2$  models.

## H.5 Observables

To estimate any scalar observable of form  $\mathbf{Y}(t) = y(\mathbf{X}(t))$  in classic quantum mechanics one needs to calculate:

$$\langle \mathbf{Y} \rangle_t = \int_{\mathcal{M}} \overline{\psi(x, t)} y(x) \psi(x, t) dx.$$

In our setup, we can calculate this using the samples  $X_{[\frac{Nt}{T}]} \approx X(t) \sim |\psi(\cdot, t)|^2$ :

$$\langle \mathbf{Y} \rangle_t \approx \frac{1}{B} \sum_j^B y(X_{[\frac{Nt}{T}]_j}),$$

where  $B \geq 1$  is the batch size,  $N$  is the time discretization size. The estimation error has magnitude  $\mathcal{O}(\frac{1}{\sqrt{B}} + \epsilon + \varepsilon)$ , where  $\epsilon = \frac{T}{N}$  and  $\varepsilon$  is the  $L_2$  error of recovering true  $u, v$ . In our paper, we have not bounded  $\varepsilon$  but provide estimates for it in our experiments against the finite difference solution.<sup>7</sup>

## H.6 Wave-function

Recovering the wave function from  $u, v$  is possible using a relatively slow procedure. Our experiments do not cover this because our approach's main idea is to avoid calculating wave function. But for the record, it is possible. Assume we solved equations for  $u, v$ . We can get the phase and density by integrating (35):

$$S(x, t) = S(x, 0) + \int_0^t \left( \frac{1}{2m} \langle \nabla, u(x, t) \rangle + \frac{1}{2\hbar} \|u(x, t)\|^2 - \frac{1}{2\hbar} \|v(x, t)\|^2 - \frac{1}{\hbar} V(x, t) \right) dt, \quad (51)$$

$$\rho(x, t) = \rho_0(x) \exp \left( \int_0^t \left( -\langle \nabla, v(x, t) \rangle - \frac{2m}{\hbar} \langle u(x, t), v(x, t) \rangle \right) dt \right) \quad (52)$$

This allows us to define  $\psi = \sqrt{\rho(x, t)} e^{iS(x, t)}$ , which satisfies the Schrödinger equation (1).

Suppose we want to estimate it over a grid with  $N$  time intervals and  $\lceil \sqrt{N} \rceil$  intervals for each coordinate (a typical recommendation for Equation (1) is to have a grid satisfying  $dx^2 \approx dt$ ). It leads to a sample complexity of  $\mathcal{O}(N^{\frac{d}{2}+1})$ , which is as slow as other grid-based methods for quantum mechanics. The error in that case will also be  $\mathcal{O}(\sqrt{\epsilon} + \varepsilon)$  [58].

## H.7 Ground state

Unfortunately, our approach is unsuited for the ground state estimation or any other stationary state. FermiNet [26] does a fantastic job already. The main focus of our work is time evolution. It is possible to estimate some observable  $\mathbf{Y}$  for the ground state if its energy level is unique and significantly lower than others. In that case, the following value approximately equals the group state observable for  $T \gg 1$ :

$$\langle \mathbf{Y} \rangle_{\text{ground}} \approx \frac{1}{T} \int_0^T \langle \mathbf{Y} \rangle_t dt \approx \frac{1}{NB} \sum_{i=1}^N \sum_{j=1}^B y(X_{ij})$$

<sup>7</sup>If we are able to reach  $\mathcal{L}(\theta) = 0$  then essentially  $\varepsilon = 0$ . We leave bounding  $\varepsilon$  by  $\mathcal{L}(\theta_\tau)$  for future work.

This works only if the ground state is unique, and the initial conditions satisfy  $\int_{\mathcal{M}} \overline{\psi_0} \psi_{\text{ground}} dx \neq 0$ , and its energy is well separated from other energy levels. In that scenario, oscillations will cancel each other out.

## I Future work

This section discusses possible directions for future research. Our method is a promising direction for fast quantum mechanics simulations, but we consider the most straightforward setup in our work.

Possible future advances include:

- In our work, we consider the simplest integrator of SDE (Euler-Maruyama), which may require setting  $N \gg 1$  to achieve the desired accuracy. However, a higher-order integrator [58] or an adaptive integrator [59] should achieve the desired accuracy with much lower  $N$ .
- It should be possible to extend our approach to a wide variety of other quantum mechanical equations, including Dirac and Klein-Gordon equations used to account for special relativity [21, 60], a non-linear Schrödinger (1) equation used in condensed matter physics [61] by using McKean-Vlasov SDEs and the mean-field limit [62, 63, 24], and the Shrödinger equation with a spin component [64, 65].
- We consider a rather simple, fully connected architecture of neural networks with tanh activation and three layers. It might be more beneficial to consider specialized architectures for quantum mechanical simulations, e.g., [26].
- Many practical tasks require knowledge of the error magnitude. Thus, providing explicit bounds on  $\varepsilon$  in terms of  $\mathcal{L}(\theta_M)$  is critical.